ACS SENSORS

pubs.acs.org/acssensors Article

VOC Mixture Sensing with a MOF Film Sensor Array: Detection and Discrimination of Xylene Isomers and Their Ternary Blends

Peng Qin, Brian A. Day, Salih Okur, Chun Li, Abhinav Chandresh, Christopher E. Wilmer, and Lars Heinke*

Cite This: https://doi.org/10.1021/acssensors.2c00301 Read Online

ACCESS | Metrics & More | Article Recommendations | Supporting Information

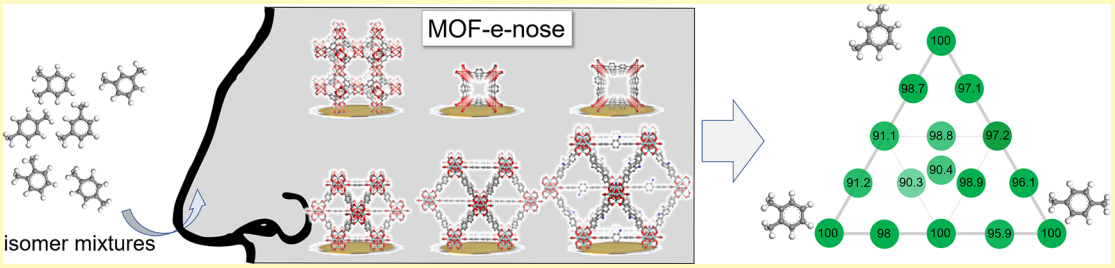

ABSTRACT: Detection and recognition of volatile organic compounds (VOCs) are crucial in many applications. While pure VOCs can be detected by various sensors, the discrimination of VOCs in mixtures, especially of similar molecules, is hindered by cross-sensitivities. Isomer identification in mixtures is even harder. Metal−organic frameworks (MOFs) with their well-defined, nanoporous, and versatile structures have the potential to improve the VOC sensing performance by tailoring the adsorption affinities. Here, we detect and identify ternary xylene isomer mixtures by using an array of six gravimetric, quartz crystal microbalance (QCM)-based sensors coated with selected MOF films with different isomer affinities. We use classical molecular simulations to provide insights into the sensing mechanism. In addition to the attractive interaction between the analytes and the MOF film, the isomer discrimination is caused by the rigid crystalline framework sterically controlling the access of the isomers to different adsorption sites in the MOFs. The sensor array has a very low limit of detection of 1 ppm for each pure isomer and allows the isomer discrimination in mixtures. At 100 ppm, 16 different ternary *o*−*p*−*m*-xylene mixtures were identified with high classification accuracy (96.5%). This work shows the unprecedented performance of MOF-sensor arrays, also referred to as MOF-electronic nose (MOF-e-nose), for sensing VOC mixtures. Based on the study, guidelines for detecting and discriminating complex mixtures of volatile molecules are also provided.

KEYWORDS: *sensors, electronic nose, metal−organic frameworks, xylene, ternary mixtures*

Clean air and the detection of pollution are of utmost importance for human health. Many common air pollutants are characterized as volatile organic compounds (VOCs), including benzene, toluene, and xylene.[1] Therefore, the realization of reliable and practical VOC sensors is very important. Due to its chemical similarities, its low reactivities, and low required limits of detection, the efficient recognition and discrimination of VOCs present a great scientific and technical challenge.[2] Usually, VOCs occur in mixtures of different molecules with different hazardous potentials.[3] The precise sensing of such complex mixtures is an unsolved problem, especially when the mixture is composed of molecules with similar physical properties, like molecular isomers.

Xylene has three isomeric forms, which are 1,2-dimethylbenzene, 1,3-dimethylbenzene, and 1,4-dimethylbenzene, referred to as *o*-xylene, *m*-xylene, and *p*-xylene, respectively (Figure 1a).[4] Xylene is an important chemical feedstock, finding widespread use not only in the large-scale synthesis of various polymers like polyethylene terephthalate (PET) and parylene but also in the printing, rubber, and leather industries.[5,6] Like many VOCs, at certain concentrations, xylene is harmful to human health. The US-American National Institute of Occupational Safety and Health (NIOSH) generally recommends a limit for long-term exposure of 100 ppm for xylene.[7] Although having similar structures and physical properties, the three xylene isomers have different metabolic pathways in the human and mammal body.[8] In animal tests with mice, the lethal concentration for 50% of the animals was 5,267 ppm, 4,595 ppm, and 3,907 ppm for *m*-

Received: February 9, 2022
Accepted: May 13, 2022

(a)

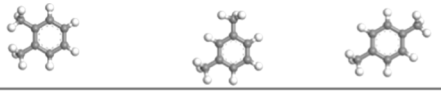

	o-xylene	*m*-xylene	*p*-xylene
T_{boil} / °C	144.42	139.10	138.35
p_{vapor} / kPa	0.87	1.11	1.17
ρ / g mL^{-1}	0.88	0.86	0.86

(b)

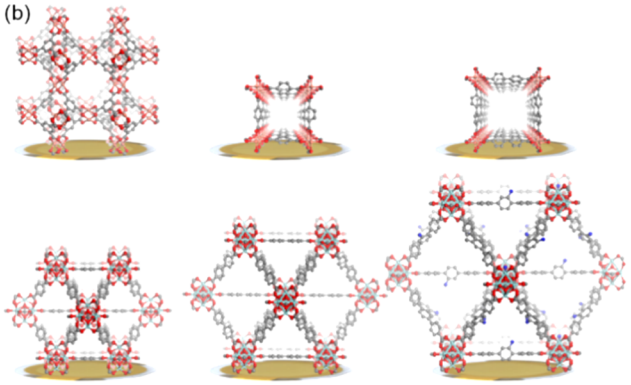

(c)

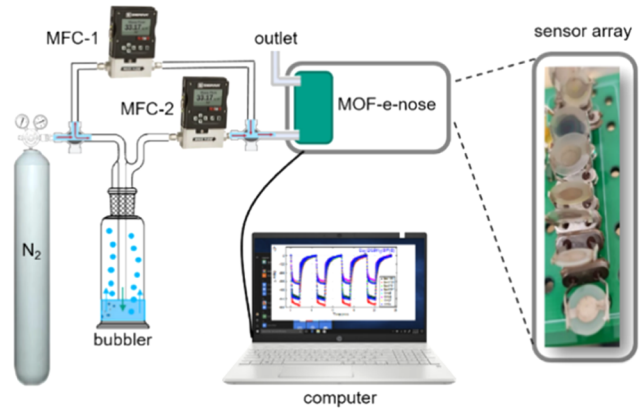

Figure 1. (a) Isomers of xylene. Important physical properties are given, i.e., temperature of the boiling point at atmospheric pressure T_{boil}, the vapor pressure at a temperature of 25 °C p_{vapor}, and the density at 25 °C ρ. (b) Structure of the MOF thin films. Top row: HKUST-1, Cu(BDC), and Cu(BPDC). Bottom row: UiO-66, UiO-67, and UiO-68-NH_2 (left to right). The color code of the atoms is C, gray; H, white (not shown for the MOFs); O, red; N, blue; Cu, orange; and Zr, cyan. (c) Sketch of the setup. The electronic nose system is composed of an array of QCM sensors coated with MOF films of six different structures. The xylene vapor concentration is controlled by the flow rates through the mass flow controller (MFC-1 and MFC-2). The sensor array is located in a gas flow chamber with an inner diameter of 15 mm and a length of 35 mm.

xylene, *o*-xylene, and *p*-xylene, respectively.[9] Hence, the detection and discrimination of xylene isomers are very important for environmental monitoring and medical care.

The standard analytical method for xylene isomer detection is based on high-resolution gas chromatography (GC).[10,11] In addition to being expensive, laborious, and time-consuming, a complex preconcentration sampling process is often required before GC analysis. In previous studies, different cost-effective methods for detecting xylene have been developed, such as mass sensor arrays,[12] chemical sensor arrays,[13] metal oxide-based sensor semiconductors,[14−16] and catalytic luminescence sensor arrays.[17] For example, oxide-nanowire-based sensors working at 400 °C were used for sensing *p*-xylene with a detection limit of 5 ppm.[15] Using a semiconducting-copolymer-based field-effect-transistor sensor, the individual xylene isomers were detected and identified at a concentration of 40 ppm.[18] While the pure isomers can be identified, distinguishing different binary and ternary xylene mixtures could not be realized. So far, the classification of ternary mixtures of xylene isomers or of other ternary VOC isomers has not yet been demonstrated.

Due to their large specific surface area, their well-defined structure, and their tunability, metal−organic frameworks (MOFs) have the potential to improve the performance of VOC sensors.[19−27] MOFs are crystalline porous materials with periodic network structures formed by self-assembly of metal nodes and organic linkers.[28,29] Several MOFs with good performance for adsorption and separation of xylene isomers have been developed. For example, several MOF-5-based structures with different selectivities have been developed for the separation of xylene isomers by gas chromatography and gas adsorption.[30] The separation of xylene isomers was also achieved by refining the pore size or by tuning the interaction with the MOF metal nodes.[31,32] These studies have focused on the separation of xylene isomers, and the discrimination and detection of xylene isomers have not yet been developed.

For VOC sensing, gravimetric transducers like quartz crystal microbalances (QCMs) have proven to be useful.[33−35] QCMs have the advantages of a simple setup, low cost, high sensitivity, and short response time.[36] The recorded frequency shifts, which are proportional to the mass changes,[37] are used as sensor signals. Various compounds and materials such as metal oxides,[38] zeolites,[39] polymers,[40] macrocyclic molecules,[41] and thiols[42] have been used to modify the surface of QCM sensors with the aim of tailoring the sensor affinity. Employing MOF films as active sensing layers, mass sensors based on QCM have been used for the detection of various pure VOCs, like formaldehyde, toluene, and chiral compounds.[43−46]

Here, we present for the first time a sensing system able to detect and distinguish several unary, binary, and ternary mixtures of the xylene isomers. It is based on a sensor array, also referred to as an electronic nose (e-nose), composed of six QCM sensors coated with six different nanoporous MOF films: HKUST-1, Cu(BDC), Cu(BPDC), UiO-66, UiO-67, and UiO-68-NH_2 (see Figure 1). (The abbreviations are: BDC is benzene-1,4-dicarboxylate, BPDC is biphenyl-4,4′-dicarboxylate, HKUST stands for Hong Kong University of Science and Technology (also referred to as $Cu_3(BTC)_2$ with BTC = benzene-1,3,5-tricarboxylate), and UiO stands for Universitetet i Oslo.) We performed classical grand canonical Monte Carlo (GCMC) simulations to provide insights into the molecular level of the adsorption affinities that result in the observed isomer discrimination. With a machine learning algorithm based on the k-nearest-neighbor (kNN) analysis,[47] the sensor array can discriminate between 16 different *o*-, *p*-, and *m*-xylene mixtures with 96.5% accuracy at a concentration of 100 ppm. The detection limit is very low (1 ppm), and, worth emphasizing, the pure xylene isomers can be distinguished with acceptable accuracy, even at very low concentrations. The study demonstrates the superior performance of nanoporous crystalline materials with versatile, well-defined, and tunable structures for gravimetric VOC sensing.

https://doi.org/10.1021/acssensors.2c00301
ACS Sens. XXXX, XXX, XXX−XXX

EXPERIMENTAL SECTION

Synthesis of MOF Films. The MOF films are prepared following previously optimized synthesis protocols.[48,49] The HKUST-1, Cu-(BDC), and Cu(BPDC) MOF film samples are prepared in a layer-by-layer method, where the substrates are alternately exposed to the metal node and linker solutions.[49,50] MOF films with an HKUST-1 structure[51] are prepared from ethanolic 1 mM copper acetate and ethanolic 0.2 mM trimesic acid (BTC) solutions. Cu(BDC) MOF films are prepared from ethanolic 1 mM copper acetate and ethanolic 0.2 mM terephthalic acid (BDC) solutions.[52] Cu(BPDC) MOF films are prepared from ethanolic 1 mM copper acetate and ethanolic 0.2 mM biphenyl dicarboxylic acid (BPDC) solutions.[52] All samples are prepared in 30 synthesis cycles by using a spray method.[53] Before SURMOF syntheses, all QCM substrates are functionalized with 16-sulfanylhexadecanoic acid (MHDA) self-assembled monolayers (SAMs).

UiO-66, UiO-67, and UiO-68-NH_2 films are prepared by vapor-assisted conversion (VAC).[48] The precursor solution was composed of $ZrOCl_2$, dicarboxylic acid, and acetic acid dissolved in DMF. A solution containing a mixture of DMF and acetic acid is dropped into a glass container. Droplets of the precursor solution (50 μL) are deposited uniformly on the sensor surface. The container is then sealed and heated to 100 °C for 3 h. Finally, the samples are dried under vacuum.

X-ray diffraction analysis is performed with a Bruker D8 diffractometer. The measurements are done in the Bragg−Brentano geometry (θ–θ) with copper K_α (λ = 1.54 Å) radiation with a position-sensitive detector (LynxEye).

Scanning electron microscope (SEM) images are taken using a TESCAN VEGA3 SEM. The samples are coated with a thin (~2 nm) platinum film using the LEICA EM ACE600 system to prevent the accumulation of charge on the sample surface.

Sensor Array. The electronic nose is a homebuilt multichannel QCM system (see Figure 1c). The frequency shift of each quartz sensor with AT-cut and approximately 10 MHz resonance frequency is recorded by the computer. Each QCM sensor, purchased from JWT China, has a circular shape of approximately 10 mm diameter. The circular Ag top electrode has a diameter of approximately 6 mm and an area of 28.3 mm^2. This is the area covered by the MOF film. During the measurements, the frequency shifts of all sensors are recorded every 1−1.7 s. The entire setup is controlled by a program code written in MATLAB.

A gas flow system is used to control the gas atmosphere at the sensors. The gas flow of the carrier gas (nitrogen) is split into two streams, whose flow rates are controlled by mass flow controllers. One stream is enriched with the VOC vapor by bubbling through liquid VOCs using a gas wash bottle. (Previous dew-point experiments with the gas flow setup showed that the resulting vapor pressure is only slightly smaller than the saturated vapor pressure.[46,54]) The other stream is pure nitrogen. Then, both streams are merged and the VOC concentration can be controlled by adjusting the flow rates. For example, the pure nitrogen channel flow rate is 60 mL/min and the VOC channel passing through liquid *m*-xylene has a flow rate of 0.55 mL/min. This results in a mixed vapor concentration of 0.55/60 times the saturated vapor pressure (10,900 ppm for *m*-xylene at 25 °C), i.e., 100 ppm.

Each sensing experiment is composed of three phases. First, the sensors are in a flow of pure nitrogen and the MOF pores are empty. Then, the gas flow is instantly enriched with a constant VOC concentration. The VOC molecules adsorb in the MOF films, and the VOC uptake results in the frequency shift of the QCM sensors, which is the sensor signal. The third step is the desorption of the adsorbed VOCs in an atmosphere of pure nitrogen. The adsorption steps are 2 h. The desorption step usually had a length of 4 h to ensure all VOC molecules desorb. In the experiments, gas flows with xylene concentrations of 1, 2, 5, 10, 50, 100, 500, 1000 ppm, and maximum concentration (i.e., close to the saturated vapor concentration of approximately 10,900 ppm for *m*-xylene, 8,500 ppm for *o*-xylene, and 11,000 ppm for *p*-xylene) were used. The numbers of uptake experiments are 3 at a concentration of 1 ppm, 3 at 2 ppm, 3 at 5 ppm, 10 at 10 ppm, 3 at 50 ppm, 16 at 100 ppm (plus six experiments for the reproducibility experiment, S10), 3 at 500 ppm, 3 at 1000 ppm, and 3 at maximum concentration. All experiments were performed at room temperature.

Data Analysis. For the data analysis, the data are classified via a machine learning algorithm based on a standard k-nearest-neighbor (kNN) algorithm, using a program code written in python (see also the Associated Content).[47,55] For the kNN classification of the sensor response, 100 data points at the end of each xylene exposure period are used. This means the data at about 2 h after the beginning of the analyte exposure (i.e., right before the desorption starts) are accumulated during a time period of approximately 2.5 min. This results in 1600 data points for all 16 xylene mixtures (Figures 6c and S16), where each data point includes the frequency shift values of all six sensors. For the classification of the pure isomers (Figure 6a), 300 data points, i.e., 100 data points of each isomer, were used. The *K*-value in kNN is set to 40, corresponding to the square root of the number of points, here 1600, following a general recommendation for setting *K*.[56−58] (Varying the *K*-value by 50% did not result in a significant change of the classification results.) The kNN classification was performed using 10-fold cross-validation, with 90% of the data points used as the training set (i.e., 1440 points) and 10% as the test set (160 points). Each mixture composition is considered a separate class; this means there are 3 classes for classifying the pure isomers (Figure 6a) and 16 classes for classifying the ternary mixtures (Figure 6c).

Data analysis with standard linear discriminant analysis (LDA) is also performed.

RESULTS AND DISCUSSION

Xylene Uptake by the MOF-Coated QCM Sensor Array. The electronic nose, i.e., the sensor array, is composed of six quartz crystal microbalance (QCM) sensors coated with thin films of different MOF structures. The MOF films have structures of types HKUST-1, Cu(BDC), Cu(BPDC), UiO-66, UiO-67, and UiO-68-NH_2 (see Figure 1b). The MOF films were chosen due to their good properties regarding the pore size, stability, uptake and diffusion properties, and synthesis conditions. The X-ray diffraction patterns (Figure S1) show that all samples are crystalline and they possess the targeted structures. Moreover, the diffraction patterns show that all samples have a high degree of crystalline orientation. Cu(BDC), Cu(BPDC), and HKUST-1 MOF films are grown in the (100) crystal orientation perpendicular to the substrate surface. The UiO-MOF films are grown in the (111) orientation. The surface morphology is imaged by scanning electron microscopy (SEM) (Figure S2).

For exploring the sensor array performance, the response of the sensor array in the atmosphere of a defined xylene mixture is investigated. To this end, the QCM frequency shifts are recorded and the gas atmosphere surrounding the sensors is switched from initially pure nitrogen to nitrogen enriched with xylene (or xylene mixture) of a certain vapor pressure. The frequency shifts of each QCM sensor, which are proportional to the mass change caused by the VOC adsorption in the MOF films, are recorded. The frequency shifts are used as sensing signals. In this way, the sensor response to xylene of various concentrations, i.e., 1, 2, 5, 10, 50, 100, 500, 1000 ppm and about 10,000 ppm, was explored. In addition, the sensor response to binary and ternary mixtures at 10 and 100 ppm was explored. In total, experiments with 47 different concentrations and compositions were performed. The frequency shifts of the QCM sensor array under exposure to the pure xylene isomers with concentrations of 10 and 50 ppm

https://doi.org/10.1021/acssensors.2c00301
ACS Sens. XXXX, XXX, XXX−XXX

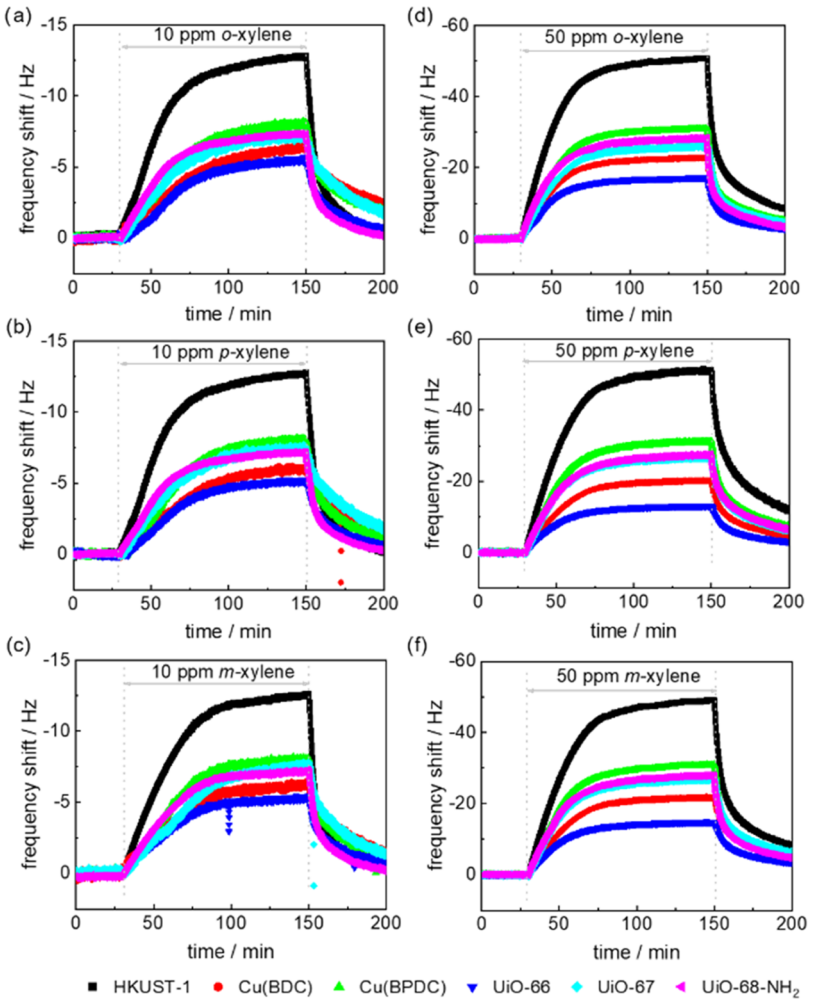

Figure 2. QCM response for the uptake of 10 ppm (a–c) and 50 ppm (d–f) xylene molecules as a function of time. The isomers and concentrations are labeled in the panels. (a, d) *o*-Xylene, (b, e) *p*-xylene, and (c, f) *m*-xylene. The color codes for the MOF sensors are black, HKUST-1; red, Cu(BDC); green, Cu(BPDC); blue, UiO-66; cyan, UiO-67; and magenta, UiO-68-NH_2.

are shown in Figure 2. Further uptake data are shown in Figures S3–S9 in the Supporting Information.

The sensor signals in equilibrium with the gas phase as a function of the pure xylene vapors of various concentrations are shown in Figure S12. The data for all MOFs and molecules can be described with single-site Langmuir isotherms. The plots show essentially linear responses in the concentration range up to 100 ppm, referred to as Henry's region.

The slopes in the linear range of the isotherm (from 0 to 500 ppm), which corresponds to the sensitivity at low concentration, are shown in Table 1. The values of the sensitivity are between approximately 0.2 and 0.9 Hz ppm^{-1}. It is noteworthy that each sensor has a different slope (i.e., sensitivity) for the same analyte. This is caused by the different absorption properties of different MOF materials and also the different amounts (or thicknesses) of the MOF films. For all xylene isomers, the HKUST-1 sensor shows the largest sensitivity, followed by Cu(BPDC). More important, some sensors show different sensitivities for the different xylene isomers. This indicates different affinities of the different isomers in the same MOF. For example, the affinity in the Henry region toward *o*-xylene is larger than for *m* and *p* in UiO-66. In UiO-67, the affinity toward *p*-xylene is highest.

Table 1. Sensitivity of the Individual Sensors Determined from Figure S12[a]

	sensitivity in Hz/ppm				
	m-xyl.	*o*-xyl.	*p*-xyl.	standard deviation in Hz	LOD in ppm
HKUST-1	0.92	0.921	0.922	0.2	0.7
Cu(BDC)	0.38	0.39	0.33	0.15	1.4
Cu(BPDC)	0.6	0.601	0.606	0.17	0.8
UiO-66	0.23	0.29	0.21	0.13	1.9
UiO-67	0.51	0.513	0.514	0.17	1.0
UiO-68-NH_2	0.53	0.527	0.532	0.17	0.9

[a]The standard deviations are determined from the baselines in Figure 2 before the analyte exposure begins (at about 20 min). The average values from the data of all six panels in Figure 2 are shown here. The LOD is calculated by 3×standard deviation divided by the sensitivity.

The calculated limits of detection (LOD; right column in Table 1) for the individual sensors range between 0.7 and 1.9 ppm, with an average value of 1.1 ppm. The estimated LOD of about 1 ppm is in agreement with the recorded data for the isomers of 1 ppm concentration (see Figure S4a–c), where the classification of the individual isomers is feasible, however, with a significant error rate (see below). Since 1 ppm is far below

https://doi.org/10.1021/acssensors.2c00301
ACS Sens. XXXX, XXX, XXX–XXX

the NIOSH-recommended long-term xylene exposure limit of 100 ppm, the sensitivity of the sensor array is sufficient.

The time response of the sensors varies with the xylene concentration. For concentrations above 50 ppm, the sensor essentially reaches the equilibrium signals within 20 min. For concentrations below 50 ppm, the sensor response was slower. No significant differences were found in the uptake rates of the individual isomers at the same concentration. We like to stress that we found in previous studies[43,46] that the vapor classification in an MOF-e-nose is already possible with very high accuracy before the final equilibrium values are reached. The response time of the sensor is governed by the uptake kinetics of the xylene molecules in the MOF films. In general, intracrystalline diffusion controls the guest uptake by MOFs, where the uptake time scales with the square of the film thickness.[59] In addition to diffusion, the mass transfer can be decelerated by defects like surface barriers, hindering the molecules from entering the pores.[59−61] In future studies, the aim is to accelerate the sensor response, e.g., by decreasing the film thickness to some extent, without significantly decreasing the sensitivity.

Simulation of the Xylene Adsorption. We used molecular simulations to better understand the affinities of the various MOFs for each of the xylene isomers. The well-defined, highly crystalline structure of the samples (see Figure S1) allows a meaningful comparison of the simulation results with the experimental findings. To this end, we performed classical GCMC adsorption simulations using the software package RASPA2.[62] Universal force field (UFF) parameters and EQeq partial charges were used for the MOFs, and OPLS parameters were used for the xylene molecules.[63−65] Due to the similarities of the xylene stereoisomers, most of the MOFs considered show closely matching adsorption behavior for all three molecules. However, Cu(BDC) and UiO-66 demonstrated the ability to favorably adsorb a subset of the xylenes, depending on the pressure of the system. Since Cu(BDC) and UiO-66 show different adsorption affinities, in agreement with the experimental data (see Table 1), the simulations focus on these MOF structures. Pure (i.e., single-component) adsorption isotherms for both MOFs are shown in Figure 3.

Our simulations show that, at low pressures, the adsorption of *o*-xylene in UiO-66 is highly preferred, and this is consistent with the predicted heats of adsorption (*o*: −72.1 ± 7.5 kJ mol^{-1}, *m*: −59.5 ± 5.4 kJ mol^{-1}, *p*: −59.6 ± 4.5 kJ mol^{-1}). UiO-66 has larger octahedral pores (∼8.9 Å) and smaller tetrahedral pores (∼3.8 Å), and snapshots from the low-pressure simulations show that *o*-xylene resides primarily in the tetrahedral pores (Figure 4a). Similarly, *m*-xylene and *p*-xylene first adsorb into the tetrahedral pores, but since it is less energetically favorable, significant loading of these pores does not occur until higher pressures than for *o*-xylene. At elevated pressures, all three isomers begin to fill the octahedral pores. At high pressures, we observe *o*-xylene double-packing octahedral pores at higher frequencies than for the other two isomers, hence the slightly higher saturation loading shown in Figure 3a. It should be noted that, while all three xylenes measure slightly longer than 3.8 Å, which is the diameter of the largest sphere that can fit in the tetrahedral pores, their aromatic centers are small enough to fit entirely in those pores, and the methyl groups can extend into the neighboring pores.

As can be seen in Figures 4b and S13, Cu(BDC) has a layered structure with spacing comparable to the length of a vertically oriented *p*-xylene. At low pressures, our simulations

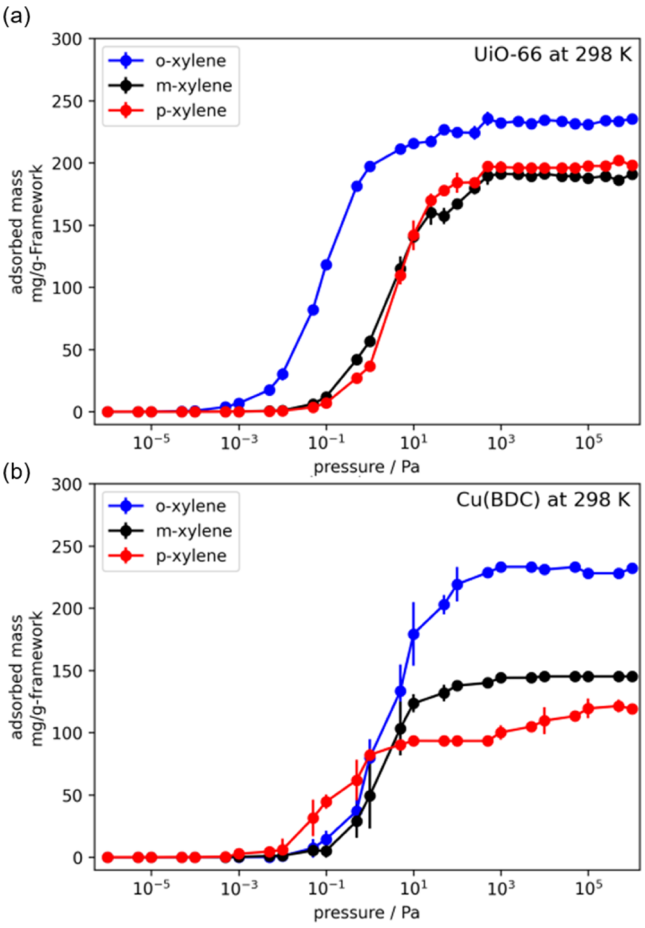

Figure 3. Simulated single-component adsorption isotherms of the xylene isomers in (a) UiO-66 and (b) Cu(BDC).

show slight preferential adsorption of *p*-xylene in this MOF, likely because it is energetically favorable for the *p*-xylene molecules to orient themselves in the pores perpendicular to the layers, stabilized by van der Waals interactions with the framework. Despite this, the heat of adsorption for *p*-xylene (−70.7 ± 4.7 kJ mol^{-1}) is only marginally larger than that for *o*-xylene (−69.0 ± 7.2 kJ mol^{-1}) and *m*-xylene (−70.2 ± 2.5 kJ mol^{-1}), but *p*-xylene is only marginally favored at low pressures, suggesting that the heat of adsorption determines the adsorption behavior at low pressures. Conversely, at high pressures, *o*-xylene is strongly favored (see Figure 3b). We attribute this to the compact arrangement of the methyl groups in *o*-xylene, allowing it to take on various orientations in the pore. Snapshots from the simulations show *o*-xylene arranged both perpendicular and parallel to the layers (see Figure S13), whereas the less compact *m*-xylene and *p*-xylene can take on fewer orientations, with the latter observed almost exclusively in the perpendicular arrangement, resulting in a net lower uptake.

The simulation data show that steric effects are fundamental for the discrimination of the isomers. While at small pressures the 9-isomers fill both pores of UiO-66, i.e., the small tetrahedral and the large octahedral pores, the filling of both pores is hindered for the *m*- and *p*-isomers, which then occupy only the small pores. Similar steric effects result in the preferential adsorption of *p*-isomer in Cu(BDC) at low pressures, compared to the other isomers. Due to the rigid crystalline framework, the steric hindrance controlling the

https://doi.org/10.1021/acssensors.2c00301
ACS Sens. XXXX, XXX, XXX−XXX

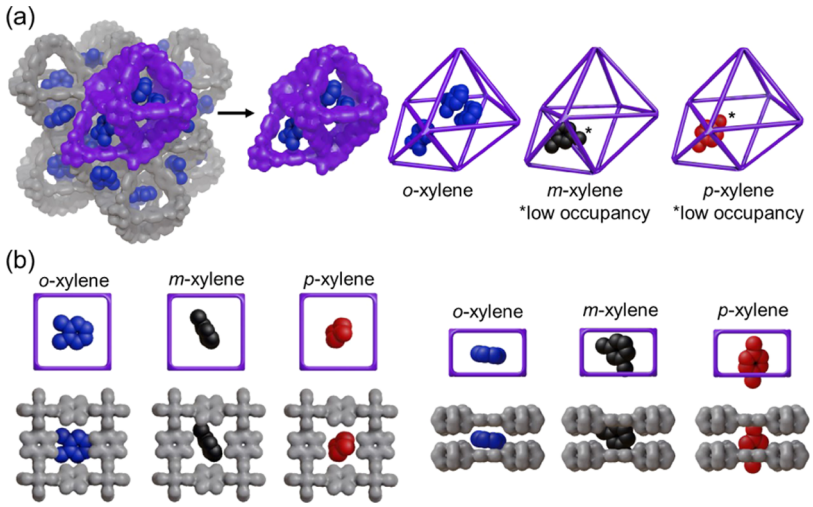

Figure 4. Snapshots of the xylene molecules in UiO-66 (a) and Cu(BDC) (b) at low pressure (0.1 Pa). For UiO-66, *o*-xylene occupies both the octahedral and tetrahedral pores, while *m*-xylene and *p*-xylene show low occupancy in the tetrahedral pores and none in the octahedral ones. For Cu(BDC), the snapshots show that *o*-xylene prefers to orient parallel to the layers, and *p*-xylene prefers to orient perpendicularly to the layers, the latter being the more energetically favorable. More data are shown in Figure S13.

access to the adsorption sites is strict. This results in a sharp cutoff controlling the size and shape of the sensed analytes. Such strict control cannot be realized by noncrystalline materials, like polymers, or by more flexible crystalline materials, such as MOF ZIF-8.

Classification of Xylene Mixtures. In addition to exploring the sensor response to the vapor of pure xylene isomers, the sensor performance for binary and ternary xylene mixtures is experimentally explored at 10 and 100 ppm, respectively. In Figures S6 and S7, the sensor signal data versus time for xylene at a total concentration of 100 ppm are shown. The *m*:*o*:*p*-xylene mixture compositions are 1:1:0, 3:1:0, 1:1:1 and 2:1:1 and permutations resulting in 13 mixtures plus 3 pure xylene vapors. The sensor response curves for all vapors (pure and blends) are qualitatively similar with small quantitative differences. Figure 5a shows the radar plots of the (final) frequency shift of the pure xylene isomers and the binary 1:1 mixtures at a concentration of 100 ppm. Radar plots for other ratios of binary mixtures and ternary mixtures are shown in Figure S11. The radar plots show that the response patterns of the different isomers are different. This means it is principally possible to distinguish *p*-, *o*-, and *m*-xylene. Moreover, the binary 1:1 mixtures also show unique patterns in the radar plot, allowing also their visual discrimination.

For comparing all mixtures, the differences in the frequency shifts relative to the average value are shown in Figure 5b for the individual sensors. The data show that the largest differences between the (pure) isomers are realized for UiO-66 and Cu(BDC) MOFs. These MOFs show the largest isomer selectivity. The maximum and minimum values (i.e., adsorption amounts) are reached for the pure vapors, and the mixture signals are within these signals. As an example, for Cu(BDC), the signal of *o*:*p* = 1:1 is in between the signals of (pure) *o*- and *p*-xylene. Moreover, the signal of *o*:*p* = 1:3 is in between the signals of pure *p*-xylene and *o*:*p* = 1:1 mixture. The same can be found for ternary mixtures. For example, for Cu(BDC), the signal of *m*:*o*:*p* = 1:2:1 is in between *m*:*o*:*p* = 1:1:1 and pure *o*-xylene. Noteworthy, the 1:1:1 ternary mixture shows a frequency response close to the average of all sensor responses, i.e., Δf_{norm} is close to 0 (see Figure 5b). The same plot as Figure 5b is expected for all concentrations within Henry's region, provided a sufficient signal-to-noise ratio exists.

To visualize the sensor performance and to quantify the accuracy of detecting and discriminating the xylene isomers and their mixtures, the sensor array data were analyzed with a machine learning algorithm; here, kNN was used. The performance of the classification by machine learning is shown in the confusion matrices, where the correct classifications are on the diagonal (in green) and false signal assignments are shown in red. The confusion matrices for the pure components are shown in Figure 6a. It shows that the isomers can be classified with perfect accuracy for high concentrations (i.e., 100 ppm and higher). For concentrations smaller than 100 ppm, a small cross-sensitivity between xylene isomers can be seen. With decreasing concentration, the classification accuracy decreases. While the classification is still acceptable at 5 and 10 ppm (approximately 77.3 and 91.2%), the classification accuracies at 1 and 2 ppm are moderate at 60.3 and 68.8%. Please note that these accuracies are significantly higher than the pure statistical assignment, which would result in 33% accuracy. The average classification accuracy as a function of vapor concentration is shown in Figure 6b.

In addition to the kNN analysis, the data were analyzed by linear discriminant analysis (LDA), shown in Figure S14. The LDA scatter plots directly display the sensor grouping and classification of xylene isomers.

For the unary, binary, and ternary mixtures at 100 ppm, the accuracy of the correct classification is shown in the ternary plot in Figure 6c. (The confusion matrix is shown in Figure S16.) It shows that all mixtures can be correctly identified by the sensor array. On average, the classification accuracy is 96.5% for distinguishing all 16 different isomer vapor mixtures. The composition of most mixtures can be identified with perfect accuracy. The smallest classification accuracy, which is still remarkable at 90.3%, is reached for the ternary mixture of *m*:*o*:*p* = 1:2:1. A detailed inspection of the confusion matrix (Figure S16) shows a small overlap of 7.6% between the *m*:*o*:*p* = 1:1:1 signal with *m*:*o*:*p* = 1:2:1 signal. Both mixtures have rather similar compositions, where the *m*:*p*-ratio is 1:1 (each

https://doi.org/10.1021/acssensors.2c00301
ACS Sens. XXXX, XXX, XXX−XXX

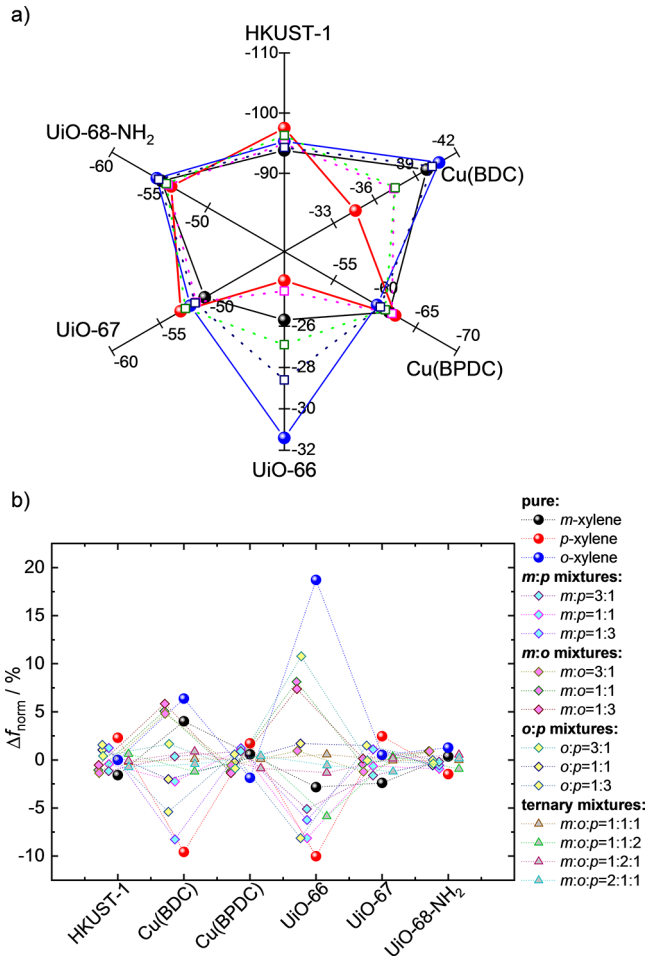

Figure 5. (a) Radar plot of the frequency shifts Δf as a response to the exposure to vapor of pure xylene isomers and binary 1:1 mixtures at 100 ppm. Please note each axis has a different scale covering 30% of the maximum value. (This means −77 to −110 Hz for HKUST-1, −29.4 to −42 Hz for Cu(BDC), −49 to −70 Hz for Cu(BPDC), −22.4 to −32 Hz for UiO-66, −42 to −60 Hz for UiO-67, and −42 to −60 UiO-68-NH_2.) (b) The relative frequency shifts of the isomers (Δf_{norm}) are shown for the pure, binary, and ternary mixture xylene vapors. Δf_{norm} is the frequency shift Δf from which the average frequency shift $\langle \Delta f \rangle$ in that sensor at 100 ppm is subtracted, divided by $\langle \Delta f \rangle$, i.e., $\Delta f_{norm} = (\Delta f - \langle \Delta f \rangle)/\langle \Delta f \rangle$. The mean values averaged over 100 points at the end of the vapor exposure step are shown. Solid spheres are pure xylene vapor, diamonds are binary mixtures (slightly shifted to the left-hand side), and triangles are ternary mixtures (slightly shifted to the right-hand side) (see the legend). The total concentrations are 100 ppm.

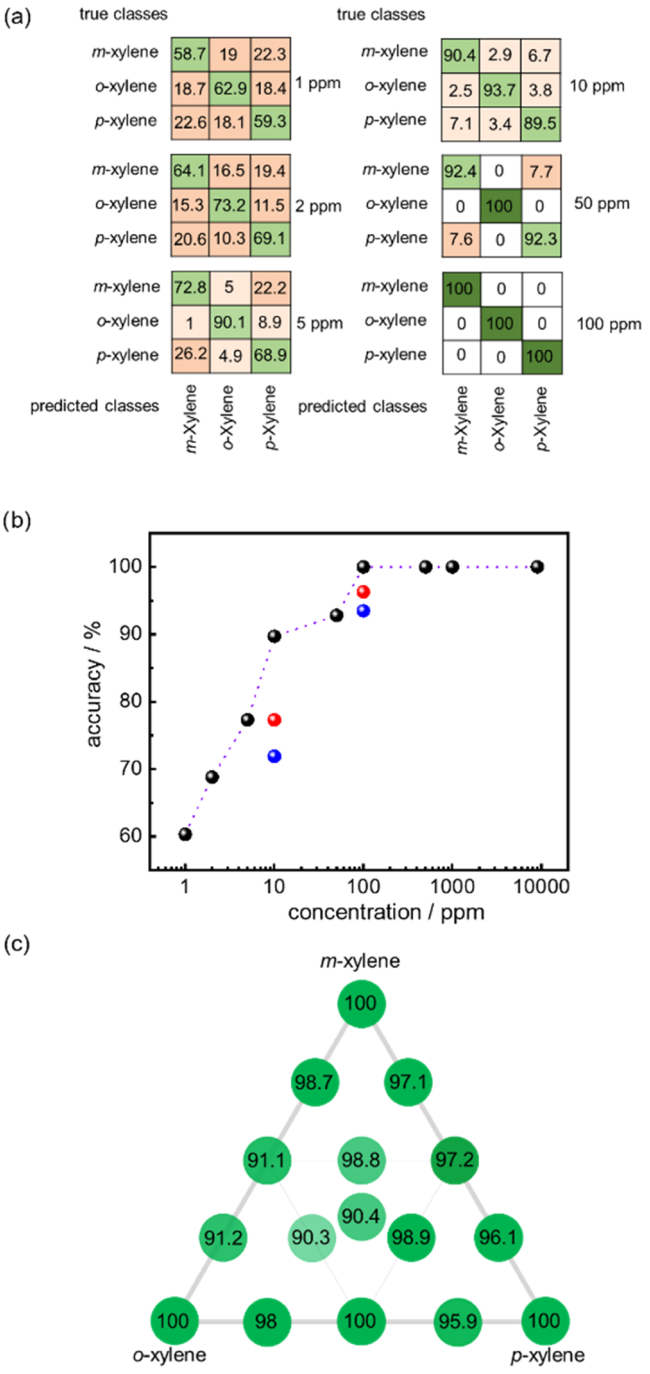

Figure 6. (a) Confusion matrices for the classification of the pure isomers at various concentrations, given on the right-hand side. (b) The average classification accuracy for different concentrations. The classification of the pure vapors is shown in black, binary 1:1 mixtures are shown in red, and ternary (including pure and binary) mixtures are shown in blue. (c) Accuracy of correctly classifying 16 different ternary xylene isomer mixtures at 100 ppm shown in a ternary plot. All numbers are given in %.

33 and 25%, respectively) and the *o*-ratio is either 33 or 50% and their precise discrimination is remarkable. To the best of our knowledge, the ability to distinguish the ternary mixtures of VOC isomers with such similar compositions has not yet been presented before.

At 10 ppm, the accuracy for the classification of the ternary mixtures is shown in Figure S15. The average accuracy (85.7%) is somewhat smaller than for 100 ppm. Nevertheless, the classification of the ternary *m*:*o*:*p* mixtures, e.g., 1:1:1 from 1:1:2, is realized with acceptable accuracy, i.e., 69.2% to 98.1%.

The sensors that show the largest isomer selectivity are UiO-66 and Cu(BDC) (see Figure 5 as well as Figures 3 and 4). Using only the data of these two sensors (Figure S17) results in a classification accuracy of the ternary xylene mixtures of 94.5% at 100 ppm and 41.1% at 10 ppm. For 100 ppm, this is slightly smaller than the accuracy based on the entire sensor array (96.5%). However, for 10 ppm, the accuracy based on the data of only two sensors is substantially reduced, compared to the entire sensor array (85.7%).

The regeneration and reproducibility of the sensor are important features of the application. Reproducibility was

https://doi.org/10.1021/acssensors.2c00301
ACS Sens. XXXX, XXX, XXX−XXX

explored by repeating the sensing experiment for three cycles (Figure S10). The results were very similar across cycles with standard deviations less than 0.5 Hz (corresponding to less than 1%), indicating the high reproducibility of the sensor performance.

The confusion matrix of the sensor data for all explored vapors from 1 ppm to saturation vapor pressure is shown in Figure S18 and that from 10 ppm to saturation vapor pressure is shown in Figure S19. The average classification accuracy for concentrations of 10 ppm and larger is 93.9%, showing that the MOF-based e-nose can not only be used to discriminate the isomers but also to discriminate the concentration of the different explored xylene vapors. While the kNN algorithm can classify the isomer composition at a certain concentration, applying the kNN analysis to all data without an assignment to the concentration (i.e., classifying the *o*-, *m*-, and *p*-isomers without information on the concentration) results in a rather poor accuracy of about 45%. There, different algorithms need to be applied.

Here, the sensor data are analyzed by classifying them according to their compositions (and concentrations) by using standard algorithms and metrics. We believe that more advanced algorithms, also based on regression allowing the estimation of composition and concentration beyond the training data, will further enhance the performance of such sensor arrays based on MOFs with defined adsorption sites and high selectivities.

CONCLUSIONS

For the detection and discrimination of xylene vapors and their ternary isomer mixtures, an electronic nose based on an array of six QCM sensors coated with different nanoporous MOF films is presented. The isomer selectivity of the sensor array is mainly based on the MOF sensors with Cu(BDC) and UiO-66 structures. Cu(BDC) exhibits an affinity for *p*-xylene at low pressures and *o*-xylene at high pressures, and UiO-66 exhibits an affinity for *o*-xylene. When combined with the data of the other MOF sensors, which have less significant isomer affinities, the electronic nose can be used to determine the composition of all three isomers in binary and ternary mixtures. At 100 ppm, the compositions of 16 ternary mixtures were determined with an average classification accuracy of 96.5%. Even at a small vapor pressure of 1 ppm, the xylene isomers can be detected and discriminated with acceptable accuracy.

The study shows that the attractive interaction between the analyte molecules and the different MOF films combined with steric effects, resulting in a size exclusion for the access to certain parts of the pore system, allows the discrimination of molecular mixtures. Due to the rigid crystalline structure, the cutoff for the size exclusion is very sharp and results in a clear distinction of the isomers. We foresee that extending the e-nose with further MOFs with distinguished affinities and pore sizes will expand the range of VOC mixtures, which can be precisely detected. There, tailored side pockets in rigid MOFs, for instance, in MOFs like HKUST-1 and differently functionalized UiO-type-MOFs, will allow us to tune the shape and size exclusion.

In the future, the detection and discrimination performance of the MOF-e-nose in a humid environment need to be explored. There, moisture-stable MOFs, whose uptake amounts are not affected by water exposure, have to be used, while MOFs like HKUST-1[60] and UiO-67,[66] whose adsorption capacity decreases upon water exposure, are not suitable. Fortunately, the MOF structures, which are the key to the xylene discrimination here, i.e., UiO-66 and Cu(BDC), have demonstrated a stable uptake and release performance, which is not impeded by exposure to moisture.[66,67] So, these MOFs can be used to explore their sensing performance in a more realistic environment. Thus, the tailored MOF-e-noses can be an excellent alternative to existing complex systems for determining VOC mixture composition in environmental monitoring and noninvasive diagnostics and it provides a promising solution for artificial olfactory systems.

ASSOCIATED CONTENT

Supporting Information

The Supporting Information is available free of charge at https://pubs.acs.org/doi/10.1021/acssensors.2c00301.

Xylene-e-MOF-nose_SI.pdf. Simulation details as well as further XRD, SEM, and QCM data;

the data (frequency shift versus time for the individual sensors; see file 1 ppm o-xylene.xlsx etc.) and the Python code for the data analysis (file: xylene-e-nose.ipynb) can be found here: https://github.com/HeinkeLab/xylene-e-nose (PDF)

AUTHOR INFORMATION

Corresponding Author

Lars Heinke − *Karlsruhe Institute of Technology (KIT), Institute of Functional Interfaces (IFG), 76344 Eggenstein-Leopoldshafen, Germany;* orcid.org/0000-0002-1439-9695; Email: Lars.Heinke@kit.edu

Authors

Peng Qin − *Karlsruhe Institute of Technology (KIT), Institute of Functional Interfaces (IFG), 76344 Eggenstein-Leopoldshafen, Germany*

Brian A. Day − *Department of Chemical & Petroleum Engineering, University of Pittsburgh, Pittsburgh, Pennsylvania 15261, Unites States;* orcid.org/0000-0003-3769-6462

Salih Okur − *Karlsruhe Institute of Technology (KIT), Institute of Functional Interfaces (IFG), 76344 Eggenstein-Leopoldshafen, Germany*

Chun Li − *Karlsruhe Institute of Technology (KIT), Institute of Functional Interfaces (IFG), 76344 Eggenstein-Leopoldshafen, Germany*

Abhinav Chandresh − *Karlsruhe Institute of Technology (KIT), Institute of Functional Interfaces (IFG), 76344 Eggenstein-Leopoldshafen, Germany*

Christopher E. Wilmer − *Department of Chemical & Petroleum Engineering, University of Pittsburgh, Pittsburgh, Pennsylvania 15261, Unites States; Department of Electrical & Computer Engineering, University of Pittsburgh, Pittsburgh, Pennsylvania 15261, Unites States;* orcid.org/0000-0002-7440-5727

Complete contact information is available at: https://pubs.acs.org/10.1021/acssensors.2c00301

Author Contributions

P.Q. performed the experiments and analyzed the data with the support of S.O. P.Q. and C.L. prepared the MOF films. A.C. measured the SEM images. B.A.D. and C.E.W. performed the simulation. L.H. planned the project and the experiments. P.Q.

https://doi.org/10.1021/acssensors.2c00301
ACS Sens. XXXX, XXX, XXX−XXX

and L.H. wrote the manuscript. All authors supported and approved the manuscript.

Notes

The authors declare no competing financial interest.

■ ACKNOWLEDGMENTS

The authors acknowledge funding through the Alexander von Humboldt Foundation, the China Scholarship Council (CSC), and the Deutsche Forschungsgemeinschaft (DFG, German Research Foundation, DFG HE 7036/5). C.E.W. and B.A.D. are grateful for support from the U.S. National Science Foundation for funding via their EAGER program: CBET-1937179. C.E.W. and B.A.D. also acknowledge support from the University of Pittsburgh's Center for Research Computing for computational resources.

■ REFERENCES

(1) Kampa, M.; Castanas, E. Human health effects of air pollution. *Environ. Pollut.* **2008**, *151*, 362−367.
(2) Schmidt, K.; Podmore, I. Current Challenges in Volatile Organic Compounds Analysis as Potential Biomarkers of Cancer. *J. Biomark.* **2015**, *2015*, No. 981458.
(3) Anand, S. S.; Philip, B. K.; Mehendale, H. M. Volatile Organic Compounds. In *Encyclopedia of Toxicology*, Academic Press, 2014; pp 967−970.
(4) Ziegler-Skylakakis, K.; Fabri, J.; Graeser, U.; Simo, T. A. Xylenes. *Ullmann's Encycl. Ind. Chem.* **2000**, 4−20.
(5) Dursch, T.; Khalil, R.; Khine, A.; Mutahi, F. Toluene Methylation to Para-xylene. *Senior Des. Rep.* **2009**, *7*, 2−4.
(6) Tsai, T.; Liub, S.-B.; Wangc, I. Disproportionation and transalkylation of alkylbenzenes over zeolite catalysts. *Appl. Catal., A* **1999**, *181*, 355−398.
(7) NIOSH, N. I. f. O. S. a. H.. NIOSH Pocket Guide to Chemical Hazards. *Cincinnati* **2007**, 335−337.
(8) Wexler, P. *Encyclopedia of Toxicology*, 3rd ed.; Elsevier/Academic Press, 2014; Vol. *1*, pp 989−993.
(9) Bonnet, P.; Raoult, G.; Gradiski, D. Lethal concentration of 50 main aromatic hydrocarbons. *Arch. Mal. Prof.* **1979**, *40*, 805−810.
(10) Baghani, A. N.; Rostami, R.; Arfaeinia, H.; Hazrati, S.; Fazlzadeh, M.; Delikhoon, M. BTEX in indoor air of beauty salons: Risk assessment, levels and factors influencing their concentrations. *Ecotoxicol. Environ. Saf.* **2018**, *159*, 102−108.
(11) Kniemeyer, O.; Fischer, T.; Wilkes, H.; Glockner, F. O.; Widdel, F. Anaerobic degradation of ethylbenzene by a new type of marine sulfate-reducing bacterium. *Appl. Environ. Microbiol.* **2003**, *69*, 760−768.
(12) Dickert, F. L.; Hayden, O.; Zenkel, M. E. Detection of Volatile Compounds with Mass-Sensitive Sensor Arrays in the Presence of Variable Ambient Humidity. *Anal. Chem.* **1999**, *71*, 1338−1341.
(13) Wang, F.; Yang, Y.; Swager, T. M. Molecular recognition for high selectivity in carbon nanotube/polythiophene chemiresistors. *Angew. Chem., Int. Ed.* **2008**, *47*, 8394−8396.
(14) Kim, H. J.; Yoon, J. W.; Choi, K. I.; Jang, H. W.; Umar, A.; Lee, J. H. Ultraselective and sensitive detection of xylene and toluene for monitoring indoor air pollution using Cr-doped NiO hierarchical nanostructures. *Nanoscale* **2013**, *5*, 7066−7073.
(15) Woo, H. S.; Kwak, C. H.; Chung, J. H.; Lee, J. H. Co-doped branched ZnO nanowires for ultraselective and sensitive detection of xylene. *ACS Appl. Mater. Interfaces* **2014**, *6*, 22553−22560.
(16) Hernández, S. C.; Hangarter, C. M.; Mulchandani, A.; Myung, N. V. Selective recognition of xylene isomers using ZnO-SWNTs hybrid gas sensors. *Analyst* **2012**, *137*, 2549−2552.
(17) Li, S.; Zheng, J.; Zhang, W.; Cao, J.; Li, S.; Rao, Z. Molecular recognition and quantitative analysis of xylene isomers utilizing cataluminescence sensor array. *Analyst* **2013**, *138*, 916−920.
(18) Wang, B.; Huynh, T. P.; Wu, W.; Hayek, N.; Do, T. T.; Cancilla, J. C.; Torrecilla, J. S.; Nahid, M. M.; Colwell, J. M.; Gazit, O. M.; Puniredd, S. R.; McNeill, C. R.; Sonar, P.; Haick, H. A Highly Sensitive Diketopyrrolopyrrole-Based Ambipolar Transistor for Selective Detection and Discrimination of Xylene Isomers. *Adv. Mater.* **2016**, *28*, 4012−4018.
(19) Lustig, W. P.; Mukherjee, S.; Rudd, N. D.; Desai, A. V.; Li, J.; Ghosh, S. K. Metal-organic frameworks: functional luminescent and photonic materials for sensing applications. *Chem. Soc. Rev.* **2017**, *46*, 3242−3285.
(20) Stassen, I.; Burtch, N.; Talin, A.; Falcaro, P.; Allendorf, M.; Ameloot, R. An updated roadmap for the integration of metal-organic frameworks with electronic devices and chemical sensors. *Chem. Soc. Rev.* **2017**, *46*, 3185−3241.
(21) Liang, W. B.; Wied, P.; Carraro, F.; Sumby, C. J.; Nidetzky, B.; Tsung, C. K.; Falcaro, P.; Doonan, C. J. Metal-Organic Framework-Based Enzyme Biocomposites. *Chem. Rev.* **2021**, *121*, 1077−1129.
(22) Woellner, M.; Hausdorf, S.; Klein, N.; Mueller, P.; Smith, M. W.; Kaskel, S. Adsorption and Detection of Hazardous Trace Gases by Metal-Organic Frameworks. *Adv. Mater.* **2018**, *30*, No. 1704679.
(23) Freund, P.; Senkovska, I.; Kaskel, S. Switchable Conductive MOF-Nanocarbon Composite Coatings as Threshold Sensing Architectures. *ACS Appl. Mater. Interfaces* **2017**, *9*, 43782−43789.
(24) Ricco, R.; Malfatti, L.; Takahashi, M.; Hill, A. J.; Falcaro, P. Applications of magnetic metal-organic framework composites. *J. Mater. Chem. A* **2013**, *1*, 13033−13045.
(25) Strauss, I.; Mundstock, A.; Treger, M.; Lange, K.; Hwang, S.; Chmelik, C.; Rusch, P.; Bigall, N. C.; Pichler, T.; Shiozawa, H.; Caro, J. Metal-Organic Framework Co-MOF-74-Based Host-Guest Composites for Resistive Gas Sensing. *ACS Appl. Mater. Interfaces* **2019**, *11*, 14175−14181.
(26) Vandezande, W.; Janssen, K. P. F.; Delport, F.; Ameloot, R.; De Vos, D. E.; Lammertyn, J.; Roeffaers, M. B. J. Parts per Million Detection of Alcohol Vapors via Metal Organic Framework Functionalized Surface Plasmon Resonance Sensors. *Anal. Chem.* **2017**, *89*, 4480−4487.
(27) Sturluson, A.; Sousa, R.; Zhang, Y.; Huynh, M. T.; Laird, C.; York, A. H. P.; Silsby, C.; Chang, C.-H.; Simon, C. M. Curating Metal-Organic Frameworks To Compose Robust Gas Sensor Arrays in Dilute Conditions. *ACS Appl. Mater. Interfaces* **2020**, *12*, 6546−6564.
(28) Yaghi, O. M.; O'Keeffe, M.; Ockwig, N. W.; Chae, H. K.; Eddaoudi, M.; Kim, J. Reticular synthesis and the design of new materials. *Nature* **2003**, *423*, 705−714.
(29) Kaskel, S. *The Chemistry of Metal−Organic Frameworks*; John Wiley & Sons, 2016, Vol. *1*, pp 5−7.
(30) Gu, Z.-Y.; Jiang, D.-Q.; Wang, H.-F.; Cui, X.-Y.; Yan, X.-P. Adsorption and Separation of Xylene Isomers and Ethylbenzene on Two Zn-Terephthalate Metal-Organic Frameworks. *J. Phys. Chem. C* **2010**, *114*, 311−316.
(31) Li, X.; Wang, J.; Bai, N.; Zhang, X.; Han, X.; da Silva, I.; Morris, C. G.; Xu, S.; Wilary, D. M.; Sun, Y.; Cheng, Y.; Murray, C. A.; Tang, C. C.; Frogley, M. D.; Cinque, G.; Lowe, T.; Zhang, H.; Ramirez-Cuesta, A. J.; Thomas, K. M.; Bolton, L. W.; Yang, S.; Schroder, M. Refinement of pore size at sub-angstrom precision in robust metal-organic frameworks for separation of xylenes. *Nat. Commun.* **2020**, *11*, No. 4280.
(32) Gonzalez, M. I.; Kapelewski, M. T.; Bloch, E. D.; Milner, P. J.; Reed, D. A.; Hudson, M. R.; Mason, J. A.; Barin, G.; Brown, C. M.; Long, J. R. Separation of Xylene Isomers through Multiple Metal Site Interactions in Metal-Organic Frameworks. *J. Am. Chem. Soc.* **2018**, *140*, 3412−3422.
(33) Kumar, V. R.; Gopidas, K. R. Synthesis and characterization of gold-nanoparticle-cored dendrimers stabilized by metal-carbon bonds. *Chem. Asian J.* **2010**, *5*, 887−896.
(34) Lu, H.-H.; Rao, Y. K.; Wu, T.-Z.; Tzeng, Y.-M. Direct characterization and quantification of volatile organic compounds by piezoelectric module chips sensor. *Sens. Actuators. B* **2009**, *137*, 741−746.
(35) Vashist, S. K.; Vashist, P. Recent Advances in Quartz Crystal Microbalance-Based Sensors. *J. Sens.* **2011**, *2011*, 1−13.

https://doi.org/10.1021/acssensors.2c00301
ACS Sens. XXXX, XXX, XXX−XXX

(36) Harbeck, M.; Erbahar, D. D.; Gürol, I.; Musluoğlu, E.; Ahsen, V.; Öztürk, Z. Z. Phthalocyanines as sensitive coatings for QCM sensors operating in liquids for the detection of organic compounds. *Sens. Actuators, B* **2010**, *150*, 346−354.
(37) Sauerbrey, G. Verwendung von Schwingquarzen zur Wägung dünner Schichten und zur Mikrowägung. *Z. Phys.* **1959**, *155*, 206−222.
(38) Horzum, N.; Tascioglu, D.; Özbek, C.; Okur, S.; Demir, M. M. VOC sensors based on a metal oxide nanofibrous membrane/QCM system prepared by electrospinning. *New J. Chem.* **2014**, *38*, 5761−5768.
(39) Park, J.; Tabata, H. Gas Sensor Array Using a Hybrid Structure Based on Zeolite and Oxide Semiconductors for Multiple Bio-Gas Detection. *ACS Omega* **2021**, *6*, 21284−21293.
(40) Fan, X.; Du, B. Selective detection of trace p-xylene by polymer-coated QCM sensors. *Sens. Actuators, B* **2012**, *166−167*, 753−760.
(41) Koshets, I. A.; Kazantseva, Z. I.; Shirshov, Y. M.; Cherenok, S. A.; Kalchenko, V. I. Calixarene films as sensitive coatings for QCM-based gas sensors. *Sens. Actuators, B* **2005**, *106*, 177−181.
(42) Hashemipour, S.; Yaftian, M. R.; Kalhor, H.; Ghanbari, M. A study on the discrimination of xylene isomers vapors by quartz crystal microbalance sensors. *J. Iran. Chem. Soc.* **2021**, *18*, 751−763.
(43) Okur, S.; Qin, P.; Chandresh, A.; Li, C.; Zhang, Z.; Lemmer, U.; Heinke, L. An Enantioselective e-Nose: An Array of Nanoporous Homochiral MOF Films for Stereospecific Sensing of Chiral Odors. *Angew. Chem., Int. Ed.* **2021**, *60*, 3566−3571.
(44) Haghighi, E.; Zeinali, S. Formaldehyde detection using quartz crystal microbalance (QCM) nanosensor coated by nanoporous MIL-101(Cr) film. *Microporous Mesoporous Mater.* **2020**, *300*, No. 110065.
(45) Yamagiwa, H.; Sato, S.; Fukawa, T.; Ikehara, T.; Maeda, R.; Mihara, T.; Kimura, M. Detection of volatile organic compounds by weight-detectable sensors coated with metal-organic frameworks. *Sci. Rep.* **2015**, *4*, No. 6247.
(46) Qin, P.; Okur, S.; Li, C.; Chandresh, A.; Mutruc, D.; Hecht, S.; Heinke, L. A photoprogrammable electronic nose with switchable selectivity for VOCs using MOF films. *Chem. Sci.* **2021**, *12*, 15700−15709.
(47) Güney, S.; Atasoy, A. Multiclass classification of n-butanol concentrations with k-nearest neighbor algorithm and support vector machine in an electronic nose. *Sens. Actuators, B* **2012**, *166−167*, 721−725.
(48) Virmani, E.; Rotter, J. M.; Mahringer, A.; von Zons, T.; Godt, A.; Bein, T.; Wuttke, S.; Medina, D. D. On-Surface Synthesis of Highly Oriented Thin Metal-Organic Framework Films through Vapor-Assisted Conversion. *J. Am. Chem. Soc.* **2018**, *140*, 4812−4819.
(49) Shekhah, O.; Wang, H.; Zacher, D.; Fischer, R. A.; Wöll, C. Growth mechanism of metal-organic frameworks: insights into the nucleation by employing a step-by-step route. *Angew. Chem., Int. Ed.* **2009**, *48*, 5038−5041.
(50) Heinke, L.; Wöll, C. Surface-Mounted Metal-Organic Frameworks: Crystalline and Porous Molecular Assemblies for Fundamental Insights and Advanced Applications. *Adv. Mater.* **2019**, *31*, No. e1806324.
(51) Chui, S. S.-Y.; Lo, S. M.-F.; Charmant, J. P. H.; Orpen, A. G.; Williams, I. D. A Chemically Functionalizable Nanoporous Material [Cu3(TMA)2(H2O)3]n. *Science* **1999**, *283*, 1148−1150.
(52) Liu, J.; Lukose, B.; Shekhah, O.; Arslan, H. K.; Weidler, P.; Gliemann, H.; Bräse, S.; Grosjean, S.; Godt, A.; Feng, X.; Müllen, K.; Magdau, I. B.; Heine, T.; Wöll, C. A novel series of isoreticular metal organic frameworks: realizing metastable structures by liquid phase epitaxy. *Sci. Rep.* **2012**, *2*, No. 921.
(53) Hurrle, S.; Friebe, S.; Wohlgemuth, J.; Wöll, C.; Caro, J.; Heinke, L. Sprayable, Large-Area Metal−Organic Framework Films and Membranes of Varying Thickness. *Chem. - Eur. J.* **2017**, *23*, 2294−2298.
(54) Li, C.; Zhang, Z.; Heinke, L. Mass transfer of toluene in a series of metal−organic frameworks: molecular clusters inside the nanopores cause slow and step-like release. *Phys. Chem. Chem. Phys.* **2022**, *24*, 3994−4001.
(55) Tang, K. T.; Lin, Y. S.; Shyu, J. M. A local weighted nearest neighbor algorithm and a weighted and constrained least-squared method for mixed odor analysis by electronic nose systems. *Sensors* **2010**, *10*, 10467−10483.
(56) Lall, U.; Sharma, A. A Nearest Neighbor Bootstrap For Resampling Hydrologic Time Series. *Water Resour. Res.* **1996**, *32*, 679−693.
(57) Jirina, M.; Jirina, M. Classifiers Based on Inverted Distances. In *New Fundamental Technologies in Data Mining*, IntechOpen, 2011; Vol. *1*, pp 369−387.
(58) Hart, P. E.; Stork, D. G.; Duda, R. O. *Pattern Classification*; Wiley: Hoboken, 2000.
(59) Kärger, J.; Ruthven, D. M.; Theodorou, D. N. *Diffusion in Nanoporous Materials*; Wiley-VCH, 2012; p 902.
(60) Heinke, L.; Gu, Z.; Wöll, C. The surface barrier phenomenon at the loading of metal-organic frameworks. *Nat. Commun.* **2014**, *5*, No. 4562.
(61) Heinke, L.; Kortunov, P.; Tzoulaki, D.; Kärger, J. Exchange dynamics at the interface of nanoporous materials with their surroundings. *Phys. Rev. Lett.* **2007**, *99*, No. 228301.
(62) Dubbeldam, D.; Calero, S.; Ellis, D. E.; Snurr, R. Q. RASPA: molecular simulation software for adsorption and diffusion in flexible nanoporous materials. *Mol. Simul.* **2016**, *42*, 81−101.
(63) Rappé, A. K.; Casewit, C. J.; Colwell, K. S.; Goddard, W. A.; Skiff, W. M. UFF, a Full Periodic Table Force Field for Molecular Mechanics and Molecular Dynamics Simulations. *J. Am. Chem. Soc.* **1992**, *114*, 10024−10035.
(64) Jorgensen, W. L.; Maxwell, D. S.; Tirado-Rives, J. Development and Testing of the OPLS All-Atom Force Field on Conformational Energetics and Properties of Organic Liquids. *J. Am. Chem. Soc.* **1996**, *118*, 11225−11236.
(65) Wilmer, C. E.; Kim, K. C.; Snurr, R. Q. An Extended Charge Equilibration Method. *J Phys Chem Lett* **2012**, *3*, 2506−2511.
(66) Li, C.; Chandresh, A.; Zhang, Z.; Moulai, S.; Heinke, L. Stability and Degradation of Metal−Organic-Framework Films under Ambient Air Explored by Uptake and Diffusion Experiments. *Adv. Mater. Interfaces* **2022**, *9*, No. 2101947.
(67) Hanke, M.; Arslan, H. K.; Bauer, S.; Zybaylo, O.; Christophis, C.; Gliemann, H.; Rosenhahn, A.; Wöll, C. The Biocompatibility of Metal-Organic Framework Coatings: An Investigation on the Stability of SURMOFs with Regard to Water and Selected Cell Culture Media. *Langmuir* **2012**, *28*, 6877−6884.

https://doi.org/10.1021/acssensors.2c00301
ACS Sens. XXXX, XXX, XXX−XXX